



## REINFORCEMENT-FREE DECKS USING A MODIFIED STRUT-AND-TIE MODEL: PART 1 - ANALYSIS

Journal:	<i>ACI Structural and Materials Journals</i>
Manuscript ID:	draft
Journal Name:	ACI Structural Journal
Date Submitted by the Author:	
Complete List of Authors:	BAE, HAN UG; University of Wisconsin-Madison, Civil and Environmental Engineering Oliva, Michael; University of Wisconsin-Madison, Civil and Environmental Engineering Bank, Lawrence; University of Wisconsin-Madison, Civil and Environmental Engineering
Keywords:	strut-and-tie model, reinforcement-free deck, punching shear, precast prestressed girder, bridge decks, compressive membrane action, deck analysis, wide flange concrete girder, stay-in-place formwork

# REINFORCEMENT-FREE DECKS USING A MODIFIED STRUT-AND-TIE MODEL:

## PART 1 - ANALYSIS

Han Ug Bae, Michael G. Oliva, Lawrence C. Bank

Department of Civil and Environmental Engineering, University of Wisconsin-Madison, 2205

Engineering Hall, 1415 Engineering Drive, Madison, WI 53706.

**Biography: Han Ug Bae** is a postdoctoral fellow in Civil and Environmental Engineering at University of Wisconsin-Madison. He received his BS and MS from Yonsei University, Seoul, Korea and PhD from University of Wisconsin-Madison. His research interests include strut-and-tie models, development of highway bridge design methods and bridge construction.

**Michael G. Oliva** is a Professor in the Department of Civil and Environmental Engineering at University of Wisconsin-Madison. He received his BS from University of Wisconsin-Madison; MS and PhD from University of California, Berkeley. His research interests include highway bridges, reinforced-precast-prestressed concrete design and earthquake resistance.

ACI member **Lawrence C. Bank** is a Professor in the Department of Civil and Environmental Engineering at University of Wisconsin-Madison. He received his BS from Technion- Israel Institute of Technology, Haifa, Israel; MS and PhD from Columbia University. He is a member of ACI committee 440 (Fiber Reinforced Polymer Reinforcement). His research interests include FRP composites in structural engineering, mechanics of composite materials and innovative bridge construction.

## ABSTRACT

This paper describes an application of a modified strut-and-tie model (STM) for the analysis of reinforcement-free bridge decks on concrete wide flange girders. The concept presented for the reinforcement-free bridge deck includes a combination of removing steel reinforcement, utilizing

1  
2 1 compressive membrane action in the deck by tying girders together, introducing a polypropylene  
3  
4 2 fiber to control shrinkage cracks, and the use of aggregate-coated fiber reinforced polymer planks as  
5  
6 3 stay-in-place formwork and also as a crack controlling device. A new analysis method for these  
7  
8 4 reinforcement-free decks using a modified STM that considers material and geometrical  
9  
10 5 nonlinearity is proposed. The model provides a 2D axisymmetric representation of the behavior of  
11  
12 6 the reinforcement-free deck and it is capable of capturing punching and flexural failure.  
13  
14 7 Comparisons to FEM analysis were made to verify the accuracy of the proposed analysis method.  
15  
16 8 A design procedure using the proposed model is described in the accompanying paper (Part 2).  
17  
18  
19  
20  
21  
22

23 10 **Keywords:** strut-and-tie model; reinforcement-free deck; punching shear; precast prestressed  
24  
25 11 girder; bridge decks; compressive membrane action; deck analysis; wide flange concrete girder; and  
26  
27 12 stay-in-place formwork.  
28  
29  
30  
31  
32

## 33 14 INTRODUCTION

34  
35 15 The strut-and-tie model (STM) is considered to be a powerful method for design and analysis of  
36  
37 16 disturbed or discontinuous regions (D-regions) due to geometrical or structural complexity in  
38  
39 17 concrete members. Schlaich et al.<sup>1</sup> developed the basic concepts and the detailed design method for  
40  
41 18 STM that is composed of struts and ties. Recently the STM has become a widely used method to  
42  
43 19 analyze and to design D-regions and is recognized in ACI 318.<sup>2</sup> Numerous investigations and  
44  
45 20 modifications of the method have been performed to find simple and accurate means of applying  
46  
47 21 the model.<sup>3-6</sup>  
48  
49  
50

51 22 The STM can be used for a restrained bridge deck on girders since the deck behaves like a D-region  
52  
53 23 due to concentrated forces at the girder supports and at the center of the span under a wheel load,  
54  
55 24 particularly after cracking occurs at these locations. Compressive membrane action develops in the  
56  
57 25 restrained deck, if sufficient lateral restraint is provided, and it enhances the capacity of the deck.  
58  
59  
60

26 The failure mode of the deck will likely change from a flexural failure to a punching shear failure

1  
2 1 with restraint. Lateral restraint in the deck around the loaded region inhibits rotation and translation  
3  
4 2 in the plane of the deck and leads to the enhancement of the flexural capacity of the deck.<sup>7</sup> Analysis  
5  
6 3 methods to predict the enhanced capacity of the restrained deck have been suggested by a number  
7  
8 4 of researchers.<sup>8,9</sup> These methods are only able to consider the punching failure mode, however  
9  
10 5 flexural failure can actually occur if there is insufficient lateral restraint.  
11  
12

13  
14 6 One application of compressive membrane action has been in steel-free bridge decks in Canada.<sup>10</sup>  
15  
16 7 This concept of the steel-free bridge deck includes removal of conventional steel reinforcement  
17  
18 8 from the deck to prevent concrete deterioration due to corrosion. Steel straps, externally welded at  
19  
20 9 the top of the flanges of steel girders, are used to provide lateral restraint to the deck. Fiber is added  
21  
22 10 to the concrete to control thermal and shrinkage cracks and fiber reinforced polymer rebars are  
23  
24 11 added to the concrete to control large flexural cracks.<sup>11</sup>  
25  
26  
27

28 12 Another application of compressive membrane action for bridge decks has been in a pilot bridge  
29  
30 13 using a reinforcement-free deck that was built in Wisconsin to show the feasibility of the new  
31  
32 14 proposed design approach.<sup>12</sup> A new load carrying mechanism was introduced to eliminate the  
33  
34 15 conventional steel reinforcements. The mechanism is a combination of compressive membrane  
35  
36 16 action in the deck obtained by tying girders together, utilizing the high lateral stiffness of wide  
37  
38 17 flanged concrete girders for restraint, introducing a polypropylene fiber reinforced concrete (FRC)  
39  
40 18 to control shrinkage cracks, and using aggregate coated pultruded fiber reinforced polymer (FRP)  
41  
42 19 stay-in-place (SIP) panels as deck formwork and also as a deck crack controlling system. **(Fig. 1)**  
43  
44  
45 20 In this research a modified STM was developed for the analysis of this type of reinforcement-free  
46  
47 21 bridge deck and comparisons to FEM analysis were made to verify the accuracy of the STM. The  
48  
49 22 existing methods of STM analysis according to ACI 318<sup>2</sup> can not be used directly to analyze the  
50  
51 23 restrained deck since the punching shear failure behavior of the deck is in 3 dimensions and the  
52  
53 24 existing methods can not capture the enhancement of the flexural strength depending on the degree  
54  
55 25 of restraint provided.  
56  
57  
58  
59  
60

26

## RESEARCH SIGNIFICANCE

A new method to analyze reinforcement-free bridge decks is presented. Traditional bridge deck analysis and design is based on flexural behavior, yet decks often fail in punching shear. The proposed strut-and-tie model (STM) is capable of capturing the punching and flexural failure of the restrained bridge deck while previously developed analytical models only capture one of the failure modes. The authors' approach differs from previous STMs in that 2<sup>nd</sup> order analysis was used to include geometric nonlinearity in the restrained deck. The authors believe that this new model is an effective method to replace time consuming FEM analysis.

## DEVELOPMENT OF MODIFIED STM FOR RESTRAINED CONCRETE DECKS

The STM model proposed provides a 2D axisymmetric representation of the behavior of a restrained deck. It is analyzed using 2<sup>nd</sup> order methods to include geometric nonlinearity of the deck behavior. Strength effects from the FRP SIP in the reinforcement-free deck system were not considered in this approach to make the model conservative and simple. Separate finite element analyses of bridge decks were performed using ABAQUS 6.6-1<sup>3</sup> considering material and geometrical nonlinearity to serve as an "accurate" basis of constructing and verifying the more approximate STM analysis results. Verification of the finite element modeling method was obtained by comparison with the results from a restrained deck experimental test in the laboratory.<sup>14</sup>

### Geometrical configuration of the model

The rectangular loading surface of the vehicle wheel can be transformed to an equivalent circle with the same area to solve the model in an axisymmetric configuration as shown Equation (1).

$$D = \sqrt{\frac{4bd}{\pi}} \quad (1)$$

The punched out volume of the deck is generally in a pyramidal or cone shape when punching failure of the deck occurs as shown in **Fig. 2**.

1  
2 1 The compressive and tensile stress trajectories (visible as lines in the elements in **Fig. 3**) at the  
3  
4 2 failure load level of the model along section A-A in **Fig. 2** are shown in **Fig. 3** with an STM model  
5  
6 3 superimposed. The solid lines of the STM model represent the struts in compression and the dotted  
7  
8 4 lines represent the ties in tension. A spring in the lateral direction is placed at the left and right  
9  
10 5 bottom sides of the STM, at the supports, to simulate axial restraint from adjoining structural  
11  
12 6 elements.

15  
16 7 It is possible to replace the diagonal parts of the STM shown in **Fig. 4(b)** with a single diagonal  
17  
18 8 strut as shown in **Fig. 4(a)** if the strength of the diagonal elements is known. The diagonal struts in  
19  
20 9 the model represent a half portion of the failure surface in **Fig. 2(c)** and the stiffness of the springs  
21  
22 10 at each side of the 2D STM represent the radial outward restraint stiffness from the adjoining slab  
23  
24 11 over a half of the failure line at the bottom fiber shown in **Fig. 2(a)**. The locations of the top lateral  
25  
26 12 strut and bottom end of the diagonal strut were determined from a linear bending stress distribution  
27  
28 13 for simplicity and are included in **Fig. 4(a)**. They coincided well with the location of the center of  
29  
30 14 gravity of the compressive stress distribution at these locations from the nonlinear FEM analysis  
31  
32 15 close to the failure load level.

33  
34  
35 16 The length of the diagonal strut and the angle of inclination of the diagonal strut can be calculated  
36  
37 17 from Equations (2) and (3), respectively.

$$38 \quad l_{ds} = \sqrt{\frac{1}{4} \left( L - \frac{D}{2} \right)^2 + \frac{4}{9} t^2} \quad (2)$$

$$39 \quad \theta_1 = \tan^{-1} \left\{ \frac{\frac{2}{3} t}{\frac{1}{2} \left( L - \frac{D}{2} \right)} \right\} \quad (3)$$

### 40 21 **Capacity of the diagonal strut**

41  
42  
43 22 The average width of the diagonal strut in the circumferential  $r$  direction shown in **Fig. 4(a)** can be  
44  
45 23 calculated as the average of the top and the bottom width by Equation (4).

$$w_{ds} = \frac{\pi}{4} \left( \frac{D}{2} + L \right) \quad (4)$$

The sum of the tensile forces developed at the ties of the detailed STM in **Fig. 4(b)** can be calculated from Equation (5) for the ultimate axial force applied to the diagonal strut. The spreading angle ( $\theta_2$ ) represents the actual distribution of the axial compressive stress over a wider width of material in the middle of the strut as the applied end compression spreads out. It can be found from the compressive stress trajectory using FEM analysis as shown in **Fig. 3**.

$$T = P_{usd} \tan\left(\frac{\theta_2}{2}\right) \quad (5)$$

The sum of the resisting strength capacity of the ties across a strut in the STM can be calculated by assuming that it is equal to the concrete tensile strength over the inclined crack area and adjusted by a crack length ratio found from FEM analysis as given in Equation (6).

$$T_r = f_{ct} R_1 l_{ds} w_{ds} \quad (6)$$

The axial capacity of the diagonal strut, when diagonal cracking and tension failure (punching failure) develops, can be calculated from Equation (7) by equating Equations (5) and (6).

$$P_{uds} = \frac{f_{ct} R_1 l_{ds} w_{ds}}{\tan\left(\frac{\theta_2}{2}\right)} \quad (7)$$

### Stiffness of the spring in the model

The stiffness of the lateral spring at the supports in the STM is a combination of the lateral tie stiffness, the bending stiffness of the girder about its weak axis, the torsional stiffness of the girder, and the in-plane stiffness of the adjoining slab. The components of the stiffness behave like springs in series since the deck is restrained by the girders and the girders are restrained by the ties. To be conservative, the stiffness of the spring was just calculated for the span adjacent to an external girder since the lowest lateral restraint occurs at this location. One of the two springs in the STM, the one adjacent to the internal span, is assumed to be rigid since the girder on that side has a

1 relatively rigid deck acting as a flat horizontal diaphragm as shown in **Fig. 5**. Two approximations  
 2 are made here: around one half of the bottom of the conical failure surface the restraint is taken as  
 3 similar to that on the side toward the exterior girder, around the other half the adjacent deck  
 4 material is assumed to be rigid.

5 A diagram to calculate the stiffness of the springs on the exterior side of the 2D STM is shown in  
 6 **Fig. 6**. The stiffness of the restraint springs is calculated based on the assumption that the stiffness  
 7 in the radial outward direction around the exterior half of the cone is the same as the exterior lateral  
 8 stiffness of the springs in **Fig. 5**. This assumption is judged to be conservative and it appears to be  
 9 reasonable since the shear failure will start at the location nearest to the exterior girder and then  
 10 propagate circumferentially.

11 The displacement  $\delta_l$  in **Fig. 6** represents the lateral displacement at the bottom left of the exterior  
 12 strut due to a combination of elongation of the tie, flexural displacement of the girder and torsional  
 13 rotation of the girder. The deformations are those caused by a vertical force which induces a unit  
 14 distributed load  $q$  in the radial direction in the 3D model. The sum of radial outward thrust in the  
 15 form of a single force in the 2D model can be calculated from Equation (8)

$$P_l = q \times \frac{\pi}{2} L \quad (8)$$

17 The stiffness of the spring at the bottom left side of the 2D model can be calculated from Equation  
 18 (9) by using Equation (8)

$$K_l = \frac{P_l}{\delta_l} = \frac{q \pi L}{2 \delta_l} \quad (9)$$

21 *Tension tie contribution to spring stiffness:*

22 The lateral stiffness due to the tension ties, in resisting a single vehicle wheel, can be calculated  
 23 from Equation (10) assuming that the girder is rigid. It is assumed that the tension ties for a  
 24 particular deck span are anchored on the opposite sides of the girder webs. The length of the tie is  
 25 taken as the distance from outside to outside of the webs. The tie stiffness is given in Equation (10)

$$K_{tt} = \frac{A_t E_s}{S_t (S_g + t_w)} S_w \quad (10)$$

The total transverse lateral force resisted by the ties, due to a single vehicle wheel load, can be calculated as the clear span of the deck ( $L$ ) times the unit distributed load ( $q$ ) as shown in **Fig. 7**.

The lateral displacement  $\delta_{lt}$  due to the elongation of the ties alone can be calculated by Equation (11) from the total force divided by the lateral stiffness of the tension ties.

$$\delta_{lt} = \frac{L \times q}{K_{tt}} = \frac{L S_t (S_g + t_w) q}{A_t E_s S_w} \quad (11)$$

The stiffness of the spring at the bottom left side of the 2D model due to the lateral tension ties can be calculated as shown in Equation (12) by using Equations (9) and (11)

$$K_{lt} = \frac{q \pi L}{2 \delta_{lt}} = \frac{\pi A_t E_s}{2 S_t (S_g + t_w)} S_w \quad (12)$$

*Girder bending contribution to spring stiffness:*

The lateral displacement of the girder due to the lateral weak axis bending, when the patch loads are acting as shown in **Fig. 7**, can be calculated from Equation (13). In developing this estimate the girder was assumed to be supported by the tension ties, i.e. there is no lateral displacement at the tie locations. The girder is taken as simply supported laterally at the two adjacent ties nearest to the wheel patch load. The added lateral displacement is then

$$\delta_{lgb} = \frac{qL \left( S_t^3 - \frac{L^2}{2} S_t + \frac{L^3}{8} \right)}{48 E_g I_{yg}} \quad (13)$$

The stiffness of the spring at the bottom left side of the 2D model, due to the weak axis bending of the girder, can be calculated as shown in Equation (14) by using Equations (9) and (13)

$$K_{lgb} = \frac{q \pi L}{2 \delta_{lgb}} = \frac{24 \pi E_g I_{yg}}{S_t^3 - \frac{L^2}{2} S_t + \frac{L^3}{8}} \quad (14)$$

1  
2 1 *Girder torsional contribution to spring stiffness:*

3  
4 2 Additional lateral displacement of the deck occurs due to girder torsion with the deck thrust applied  
5  
6 3 at the top flange and the tie restraint at the top of the web, creating force eccentricity. This needs to  
7  
8 4 be found by an FEM analysis for the full length of the girder, applying the unit distributed load  $q$   
9  
10 5 from a single wheel over the length  $L$  as shown in **Fig. 7**. The torsional deformations of the ends of  
11  
12 6 the girder near the abutment are assumed to be fixed since concrete diaphragms are generally used  
13  
14 7 at these locations. An example of the analysis approach is shown in **Fig. 8**.

15  
16 8 The analytical model of **Fig. 8** must include the ties and their stiffnesses as well as the girder  
17  
18 9 properties to properly model the restraints on girder deformation. The ties are assumed fixed at their  
19  
20 10 opposite ends. The lateral displacement from the FEM analysis includes the displacement from the  
21  
22 11 elongation of the ties, the weak axis bending of the girder and the torsional displacement. Only the  
23  
24 12 displacement from torsional rotation is desired. The total displacement of the girder ( $\delta_1$ ) at the  
25  
26 13 center of the loading is shown in **Fig. 9** and the torsional portion of the displacement can be found  
27  
28 14 from Equation (15).

$$\delta_{lgt} = \delta_1 - \delta_2 \quad (15)$$

29  
30 15 The stiffness of the spring at the bottom left side of the 2D model due to torsion of the girder can be  
31  
32 16 calculated by using Equation (16)

$$K_{lgt} = \frac{q\pi L}{2\delta_{lgt}} \quad (16)$$

33  
34 17 The combined stiffness of the springs in series at the bottom left side of the 2D model in **Fig. 5** can  
35  
36 18 be calculated using the individual stiffnesses as shown in Equation (17)

$$\frac{1}{K_{lm}} = \frac{1}{K_{lt}} + \frac{1}{K_{lgb}} + \frac{1}{K_{lgt}} \quad (17)$$

## 21 22 23 **Modeling the diagonal strut**

24 It is also necessary to find the effective cross-sectional area of the diagonal strut for the STM. The

1 diagonal strut portion of the STM is shown in **Fig. 10**.

2 If the depth of the horizontal compression blocks at the top (midspan) and bottom (ends) of the deck  
3 are assumed to be 1/3 of the thickness, then the width of the diagonal strut at its bottom and its top  
4 can be calculated from Equation (18)

$$w_1 = \frac{t}{3} \cos \theta_1, \quad w_2 = \frac{D}{2} \sin \theta_1 + \frac{t}{3} \cos \theta_1 \quad (18)$$

5 The average width of  $w_1$  and  $w_2$  the can be calculated from Equation (19)

$$w_{avg12} = (w_1 + w_2) / 2 \quad (19)$$

6 The average of  $w_1$  and  $w_2$  is  $w_{avg12}$ , but this is not the average width of the actual strut since it has a  
7 bottle shape (**Fig. 10**). An average width of the diagonal strut ( $w_{avg}$ ) is taken as the average of the  
8 widths at the two ends ( $w_{avg12}$ ), weighted by 0.5, added to the maximum width of the bottle shaped  
9 strut ( $w_3$ ) weighted by 0.5. The maximum width of the actual bottle shaped strut must be found  
10 from the compressive stress field using a FEM analysis.

11 The average cross-sectional area of the diagonal strut can then be calculated by Equation (20)

$$A_{ds} = w_{avg} w_{ds} \quad (20)$$

## 12 **Failure Modes**

13 The failure modes of the deck model include failure of the diagonal strut, which represents a  
14 punching failure of the deck, and failure of the top lateral strut, which represents a flexural crushing  
15 failure in the top fibers of the deck. The capacity of the diagonal strut, as controlled by tension  
16 cracking, was already estimated using Equation (7). The capacity of the top lateral strut still remains  
17 to be determined. Another possible failure mode is an instability failure prior to reaching failure  
18 stresses in the members. This occurs when the lateral restraint is relatively low, representing a  
19 flexural failure with large deflection and growth of a flexural crack to the top fiber of the deck at the  
20 center of the span. Other modes of failure, such as tie rupture or girder flexural failure, occur  
21 outside of the deck and must be considered separately.

1  
2 1 The capacity of the top lateral strut can be calculated by flexural analysis of a rectangular reinforced  
3  
4 2 concrete section with tension reinforcement only. The tension reinforcement is actually a “virtual”  
5  
6 3 concept since the lateral thrust applied at the outside of the struts actually balances the top  
7  
8 4 compression force. Assume that the virtual reinforcement does not yield at the ultimate state. In the  
9  
10 5 range of deck studies completed, the tension ties never approached their yield capacity. This served  
11  
12 6 as the basis for assuming that failure will occur in the top compression block, not in the “tie” system.  
13  
14 7 The width of concrete resisting the compression is assumed as the flexural distribution width of the  
15  
16 8 deck as given in AASHTO LRFD (2008) Table 4.6.2.1.3-1<sup>15</sup> as  $E_w = 26+6.6S$  ( $E_w = 660.4+0.55S$ )  
17  
18 9 where  $E_w$  = distribution width [in. (mm)], and  $S$  = center to center spacing of the girders [ft. (mm)].  
19  
20  
21 10 The cross-sectional area of the virtual reinforcement can be calculated from the combined lateral  
22  
23 11 stiffness of the model. The value calculated in Equation (17), however, is the stiffness in the radial  
24  
25 12 direction for half the circular cone failure surface. For transverse flexure, it is necessary to convert  
26  
27 13 to the stiffness in the transverse lateral direction only. The flexural failure (crushing of the top strut  
28  
29 14 fibers) occurs due to the transverse moment. The lateral stiffness portion of the combined lateral  
30  
31 15 stiffness over the distribution width ( $E_w$ ) can be calculated using Equation (21)  
32  
33  
34  
35  
36  
37

$$K_{lf} = K_{lm} \frac{2 E_w}{\pi L} \quad (21)$$

38 16  
39  
40  
41 17 The cross-sectional area of the virtual reinforcement ( $A_{vr}$ ), taken as steel reinforcement, can be  
42  
43 18 calculated from Equation (22).  
44  
45

$$K_{lf} = \frac{A_{vr} E_s}{L} \quad (22)$$

46  
47 19  
48  
49  
50 20 The compressive force (C) in the top portion of the section and the tensile force (T) in the virtual  
51  
52 21 reinforcement when the flexural failure occurs are shown in Equation (23)  
53  
54

$$C = 0.85 f'_c E_w a, \quad T = A_{vr} E_s \varepsilon_{vr}, \quad C = T \quad (23)$$

55 22  
56  
57  
58 23 As shown in **Fig. 4(a)**, the tie in the STM model is assumed to be at  $t/6$  above the bottom of the  
59  
60 24 deck. The strain compatibility at the ultimate state shown in **Fig. 11** gives Equation (24) assuming  
25 that concrete fails at a strain of 0.003 and the virtual reinforcement does not yield.

$$0.003 \frac{5}{6} t = (0.003 + \varepsilon_{vr}) \frac{a}{\beta_1} \quad (24)$$

$a$  and  $\varepsilon_{vr}$  can be found using Equations (23) and (24). The capacity “C” of the lateral top strut can then be found by using the calculated  $a$  and Equation (23) as shown in Equation (25).

$$P_{ults} = 0.85 f'_c E_w a \quad (25)$$

### Creating a Stable STM Model

The final step in the development of the STM model is to perform a 2nd order analysis with the calculated capacities of the truss members. Second order analysis is necessary because the resistance and stability of the STM truss model are dependent on the lateral displacements at the bottom joints. As shown in **Fig. 4(a)**, however, the model is not currently a proper truss because of the lack of triangulation.

A simple way to adjust the current truss is to make an equivalent model without a horizontal top lateral strut. This would create a stable system. The capacities and the properties of the members need to be changed as shown in **Fig. 12**. The lateral spring at the left side can be replaced with a bottom tie having an identical restraining stiffness. The failure of the deleted top lateral strut can be duplicated by giving the bottom lateral tie an identical capacity since the axial force in the top and bottom members is always the same.

### Practical use of the modified STM

A nonlinear FEM analysis was required to find a number of unknown design parameters used in the proposed model such as the spreading angle of compressive force, the ratio defined as cracked length over length of the diagonal strut, the lateral torsional displacement at the top of the girder and the maximum width of the bottle shaped strut to improve accuracy of the model. The model can be used more practically without FEM analysis if these design parameters are predefined for the practical range of configurations of members used. The appropriate design factors that can be used

1  
2 1 in analysis of reinforcement-free decks on 54 in. to 72 in. (1372mm to 1829mm) deep wide flange  
3  
4 2 (or bulb tee) concrete girders are defined elsewhere<sup>14</sup> and also presented in Part 2 of this paper.  
5  
6  
7 3

#### 9 4 FINITE ELEMENT ANALYSIS

10  
11 5 ABAQUS 6.6-1<sup>13</sup> was used to conduct FEM analyses used to verify the modified STM modeling  
12 6 method. A full model was built for the FEM analysis and the “Hex 3D stress element with the linear  
13  
14 7 geometric order option” and a “reduced integration scheme” was used to reduce the required run  
15  
16 8 time for running for the non-linear analysis. The “nonlinear effects of large displacement” option  
17  
18 9 was selected in the analyses. A FEM parametric study (varying deck span, deck depth, steel tie  
19  
20 10 spacing and tie area) was performed for concrete decks on 54in. (1372mm) deep precast bulb tee  
21  
22 11 girders used in Wisconsin (**Fig. 13**). The decks were assumed to have 4000 psi (27.56 MPa)  
23  
24 12 compressive strength and 5 lb/yd<sup>3</sup> (2.97 kg/m<sup>3</sup>) of synthetic fibers.  
25  
26  
27

28  
29  
30 13 A deck restraining factor “*R*” shown in Equation (26) was proposed to examine the behavior of the  
31  
32 14 compressive membrane action in the parametric study and for use as a basis for design. The *R*  
33  
34 15 parameter can be considered as representative of the restraint applied to the deck by the ties  
35  
36 16 between girders that can result in an increase of the deck punching shear strength.  
37  
38  
39

$$40 17 R = \frac{(\text{axial stiffness of the lateral steel tie}) \times (\text{thickness of deck})}{(\text{center to center spacing of girders}) \times (\text{spacing of lateral steel tie})} \quad (26)$$

41  
42  
43  
44 18 Ninety four FEM analyses were performed for bridges with 7.5 in. (191 mm) deep decks and 6 ft. to  
45  
46 19 10 ft. (1829 mm to 3048 mm) spacing of lateral steel ties. The clear span of the decks varied from 3  
47  
48 20 ft. to 6 ft. (914 mm to 1829 mm). The resulting *R* factor varied from 0 to 1218 lb/in<sup>2</sup> (0 to 8.40  
49  
50 21 N/mm<sup>2</sup>) representing no restraint to a very large restraint. The deck was modeled with two spans  
51  
52 22 and was assumed to be placed compositely over three girders. A typical model with 5 ft. (1524 mm)  
53  
54 23 of clear deck span, 7.5 in. (191 mm) deck depth and 6 ft. (1829 mm) spacing of lateral steel ties is  
55  
56 24 shown in **Fig. 14**.  
57  
58  
59  
60 25

## COMPARISON OF FEM AND MODIFIED STM

A parametric study on the ultimate capacity of bridge decks using the modified STM was performed for the same configurations as used in a FEM parametric study. The results for the 7.5 in. (191 mm) deep deck with a 6 ft. (1829 mm) lateral tie spacing are shown in **Fig. 15** with the results from the FEM analysis.

The comparison of the FEM and STM methods shows generally acceptable agreement for deck spans less than 6 ft. (1829mm). With the thin deck and longer deck spans, the STM model might be expected to perform less accurately because of the extremely low rise in the “truss” and the greater impact of geometric and material non-linearity on the predicted response. When the clear deck span was 6 ft. (1829 mm) the STM analysis showed 4 ~ 18% higher capacity compared to the FEM analysis. This result indicates that a safety margin may be required when designing the deck using the proposed STM or the application should be limited to shorter deck spans or girder spacings. The safety margin was considered in the selection of the design load in Part 2 of this paper.

It appears that the failure mode changes from flexure to punching shear once a certain level of restraint exists. The required amount of restraint appears to depend on the span length. It also seems that providing a small amount of restraint can appreciably increase the flexural failure capacity. As the level of restraint gets high, the addition of more restraint provides little further increase in strength. It appears that shear failure occurs when the restraint ( $R$ ) is above 600 lb/in<sup>2</sup> (4.13 N/mm<sup>2</sup>). The improvement of the ultimate strength is minimal with an increase of the deck restraining factor ( $R$ ) over 900 lb/in<sup>2</sup> (6.20 N/mm<sup>2</sup>).

The failure mode predicted by the STM matched that of the FEM analysis for the 7.5 in. (191 mm) deep deck with 3 ft., 4 ft. and 5 ft. (914 mm, 1219 mm and 1524 mm) clear deck spans. The failure mode with a 6 ft. (1829 mm) clear deck span matched that of the FEM analysis in most of the cases but the failure mode of the modified STM for the case with deck restraining factor of 174 lb/in<sup>2</sup> (1.20 N/mm<sup>2</sup>) was instability failure while that of the FEM analysis was flexural failure with crushing of the concrete at top fiber at the center of the span. The FEM analysis was also capable

1 of catching the instability failure mode but the only cases with this failure mode were where no  
2 lateral steel tie was provided ( $R = 0$ ).  
3  
4 FEM and STM analyses for a 7.5 in. (191 mm) deep deck with 8 ft. and 10ft. (2438 mm or 3048  
5 mm) lateral tie spacings were also performed. The results were similar to those shown in Fig. 15.  
6 The results indicate that for a given span length, deck thickness and deck restraining factor, the  
7 failure capacity does not change significantly with tie spacings between 6ft. and 10ft. (1829 mm  
8 and 3048 mm). The decks with the same thickness and span had the same capacity when the  
9 spacing of the ties was varied from 6ft. to 10ft. (1829 mm to 3048 mm) if the cross-sectional area of  
10 the tension ties (and axial stiffness) was modified to keep the deck restraint factor constant.  
11 Referring to Equation (26), if the deck thickness and span are kept constant, in order to keep the  
12 deck restraining factor constant the tie area must be increased in direct proportion to the tie spacing.  
13

## 14 CONCLUSIONS

15 The following conclusions may be made based on the analysis procedure for the reinforcement free-  
16 decks:

- 17 1 The proposed equivalent 2D strut-and-tie model (STM) can effectively replace the time  
18 consuming FEM analysis for predicting the capacity of a 7 in. (178 mm) or thicker  
19 restrained deck when the deck clear span does not exceed 6 ft. (1830 mm). The model is  
20 capable of capturing the punching shear failure, the failure at mid-span due to flexural  
21 crushing of concrete and instability failure. The model provides an acceptable 2D  
22 axisymmetric representation of the behavior of the restrained deck.
- 23 2 A safety margin should be included in deck strength predictions using the simple STM for a  
24 design. The predicted capacities using the STM analyses for a 7.5 in. (191 mm) deep deck  
25 matched well when the clear deck spans were between 3 ft. and 5 ft. (914 mm and 1524  
26 mm) though showing slightly unconservative results. When the clear deck span was 6 ft.  
(1829 mm) the STM analysis showed 4 ~ 18% higher capacity compared to the accurate

1  
2 1 FEM analysis. This result indicates that a safety margin may be required when designing the  
3  
4 2 deck using the proposed STM. The safety margin was considered in the selection of the  
5  
6 3 design load in Part 2 of this paper.  
7  
8

9 4 3 The new procedure using the modified strut-and-tie model can be used to design bridge  
10  
11 5 decks within the dimensions and support limits defined for this research.  
12  
13  
14 6

### 7 **ACKNOWLEDGEMENT**

18 8 This project was supported through funding provided by the Federal Highway Administration  
19  
20 9 through the Wisconsin Department of Transportation under the Innovative Bridge Research and  
21  
22 10 Construction program. The views expressed in the article are those of the authors and not the  
23  
24 11 sponsoring organizations.  
25  
26  
27  
28 12  
29  
30  
31  
32  
33  
34  
35  
36  
37  
38  
39  
40  
41  
42  
43  
44  
45  
46  
47  
48  
49  
50  
51  
52  
53  
54  
55  
56  
57  
58  
59  
60

## NOTATION

1		
2	1	
3		
4	2	$a$ = height of a Whitney equivalent rectangular compressive stress block
5		
6	3	$A_{ds}$ = the average cross-sectional area of the diagonal strut
7		
8		
9	4	$A_t$ = cross-sectional area of a single steel tension tie
10		
11		
12	5	$b$ = lateral (in perpendicular direction to the girder) length of the rectangular loading area
13		
14	6	$d$ = longitudinal (in parallel direction to the girder) length of the rectangular loading area
15		
16		
17	7	$D$ = diameter of equivalent circular loading area
18		
19	8	$E_g$ = elastic modulus of the girder
20		
21		
22	9	$E_s$ = modulus of elasticity of steel
23		
24		
25	10	$f_{ct}$ = tensile strength of the deck given by $5\sqrt{f'_c}$ psi ( $0.415\sqrt{f'_c}$ MPa), $\sqrt{f'_c}$ in psi (MPa)
26		
27		
28	11	$I_{yg}$ = weak axis moment of inertia of the girder
29		
30		
31	12	$K_l$ = the stiffness of the spring at the bottom left side of the 2D model
32		
33		
34	13	$K_{lf}$ = lateral portion of the combined lateral stiffness
35		
36		
37	14	$K_{lgb}$ = the stiffness of the spring at the bottom left side of the 2D model due to weak axis
38		
39		
40	15	bending of the girder
41		
42	16	$K_{lgt}$ = the stiffness of the spring at the bottom left side of the 2D model due to torsion of the
43		
44		
45	17	girder
46		
47		
48	18	$K_{lm}$ = the stiffness of the spring at the bottom left side of the 2D model
49		
50		
51	19	$K_{lt}$ = stiffness of the spring at the bottom left side of the 2D model representing the lateral
52		
53	20	tension tie contribution to the restraint
54		
55		
56	21	$K_{tt}$ = the lateral stiffness of the tension ties resisting a single vehicle wheel
57		
58	22	$l_{ds}$ = the length of the diagonal strut
59		
60		
	23	$L$ = deck clear span between girders

1			
2	1	$P_l$	= a sum of radial outward thrust in the form of a single force in the 2D model
3			
4	2	$P_{usd}$	= capacity of the diagonal strut
5			
6			
7	3	$P_{utls}$	= capacity of the lateral top strut
8			
9			
10	4	$q$	= unit distributed thrust around the 3D cone
11			
12	5	$R$	= deck restraining factor
13			
14			
15	6	$R_1$	= a ratio of (cracked length found from FEM)/ $l_{ds}$
16			
17			
18	7	$S_t$	= spacing of the tension ties
19			
20			
21	8	$S_g$	= center to center spacing of the girders
22			
23			
24	9	$S_w$	= the spacing of the vehicle axle and wheels in a longitudinal (parallel direction to the
25			
26	10		girder) direction
27			
28	11	$t$	= deck thickness
29			
30			
31	12	$t_w$	= thickness of the web of the girder
32			
33			
34	13	$T$	= sum of tensile force in the ties
35			
36	14	$T_r$	= sum of resisting capacity of the ties
37			
38			
39	15	$w_{avg12}$	= the average width of $w_1$ and $w_2$
40			
41			
42	16	$w_{ds}$	= the width of the diagonal strut around half the circumference of the failure cone, in the $r$
43			
44	17		direction
45			
46			
47	18	$w_1$	= the width of the diagonal strut at its bottom
48			
49	19	$w_2$	= the width of the diagonal strut at its top
50			
51			
52	20	$\beta_1$	= a factor relating the depth of equivalent rectangular compressive stress block to the
53			
54	21		neutral axis depth
55			
56			
57	22	$\delta_l$	= the lateral displacement in the STM model due to the elongation of the restraints
58			
59			
60	23	$\delta_{lgb}$	= lateral displacement due to bending of the girder in its weak axis

- 1  
2 1  $\delta_{igt}$  = the lateral torsional displacement at the top of the girder  
3  
4 2  $\delta_{lt}$  = the lateral displacement in STM model due to the elongation of the tie  
5  
6  
7 3  $\delta_1$  = lateral displacement at the loading location  
8  
9  
10 4  $\delta_2$  = lateral displacement at the shear center of the girder  
11  
12  
13 5  $\varepsilon_{vr}$  = strain in the virtual reinforcement  
14  
15 6  $\theta_1$  = angle of inclination of the diagonal strut  
16  
17  
18 7  $\theta_2$  = spreading angle of the compressive force  
19  
20  
21  
22  
23  
24  
25  
26  
27  
28  
29  
30  
31  
32  
33  
34  
35  
36  
37  
38  
39  
40  
41  
42  
43  
44  
45  
46  
47  
48  
49  
50  
51  
52  
53  
54  
55  
56  
57  
58  
59  
60

## REFERENCES

1. Schlaich, J.; Schafer, K.; and Jennewein, M., "Towards a Consistent Design of Structural Concrete," *Journal of the Prestressed Concrete Institute*, V. 32, 1978, pp. 74-150.
2. ACI Committee 318, "Building Code Requirements for Structural Concrete (ACI 318-05) and Commentary (318R-05)," American Concrete Institute, Farmington Hills, Mich., 2005, 430 pp.
3. Tan, K. H., "Size Effect on Shear Strength of Deep Beams: Investigating with Strut-and-Tie Model," *Journal of the Structural Engineering*, ASCE, V. 132, No. 5, 2006, pp. 673-685.
4. Brena, S. F., and Morrison, M. C., "Factors Affecting Strength of Elements Designed using Strut-and-Tie Models," *ACI Structural Journal*, V.104, No. 3, 2007, pp. 267-277.
5. Ley, M. T.; Riding, K. A.; Widiyanto.; Bae, S.; and Breen, J. E., "Experimental Verification of Strut-and-Tie Model Design Method," *ACI Structural Journal*, V. 104, No. 6, 2007, pp. 749-755.
6. Park, J., and Kuchma, D., "Strut-and-tie Model Analysis for Strength Prediction of Deep Beams," *ACI Structural Journal*, V. 104, No. 6, 2007, pp. 657-666.
7. Hewitt, B. E., and Batchelor, B. deV., "Punching Shear Strength of Restrained Slabs," *Journal of Structural Division*, ASCE, V. 101, No. ST9, 1975, pp. 1837-1853.
8. Kuang, J. S., and Moley, C. T., "A Plasticity Model for Punching Shear of Laterally Restrained Slabs with Compressive Membrane Action," *International Journal of Mechanical Sciences*, V. 32, No. 5, 1993, pp. 371-385.
9. Mufti, A. A., and Newhook, J. P., "Punching Shear Strength of Restrained Concrete Bridge Deck Slabs," *ACI structural journal*, V. 95, No. 4, 1998, pp. 375-381.
10. Mufti, A. A.; Bakht, B.; and Jaeger, L. G., "Fiber FRC Deck Slabs with Diminished Steel Reinforcement," *IABSE Symposium Proceedings (Leningrad)*, 1991, pp. 388-389.
11. Mufti, A. A.; Jaeger, L. G.; Bakht, B.; and Wegner, L. D., "Experimental Investigation of Fibre-reinforced Concrete Deck Slabs without Internal Steel Reinforcement," *Canadian Journal of Civil Engineering*, V. 20, No. 3, Jun, 1993, pp. 398-406

1  
2  
3  
4  
5  
6  
7  
8  
9  
10  
11  
12  
13  
14  
15  
16  
17  
18  
19  
20  
21  
22  
23  
24  
25  
26  
27  
28  
29  
30  
31  
32  
33  
34  
35  
36  
37  
38  
39  
40  
41  
42  
43  
44  
45  
46  
47  
48  
49  
50  
51  
52  
53  
54  
55  
56  
57  
58  
59  
60

12. Oliva, M.G.; Bae, H.; Bank, L.C.; Russell, J.S.; Carter, J.W.; and Becker, S., "Design and Construction of a Reinforcement Free Concrete Bridge Deck on Precast Bulb Tee Girders," *Proceedings 2007 PCI/FHWA National Bridge Conference*, Phoenix, AZ, October 21-24, 2007, CD-ROM.
13. Hibbitt, Karlsson & Sorensen Inc., "ABAQUS User's manual," Hibbitt, Karlsson & Sorensen Inc., Pawtucket, RI, USA, 2004.
14. Bae, H., "Design of Reinforcement-free Bridge Decks with Wide Flange Prestressed Precast Girders," PhD Thesis, University of Wisconsin, Madison, WI, 2008.
15. AASHTO., *AASHTO LRFD Bridge Design Specifications*, 4th Ed., American Association of State Highway and Transportation Officials, Washington, D.C., 2008.

**FIGURES****List of Figures:**

**Fig. 1** – Reinforcement-free deck concept.

**Fig. 2** – Failure shape of the punching shear failure at the deck: (a) Plan view of the deck and girder; (b) Section A-A; and (c) Punched out volume

**Fig. 3** – Stress trajectory and STM of the deck: (a) Compressive stress trajectory; and (b) Tensile stress trajectory.

**Fig. 4** – Strut-and-tie-model: (a) Simplified STM for the restrained deck with boundary condition; and (b) Detailed STM of diagonal strut.

**Fig. 5** – Diagram of the lateral stiffness for the STM; (a) Plan view of the deck and girder; and (b) Components of lateral stiffness.

**Fig. 6** – Diagrams to calculate the spring stiffness of the STM: (a) 3D model; and (b) 2D model.

**Fig. 7** – Distribution of the lateral load acting on the girder.

**Fig. 8** – FEM analysis of the girder to find the lateral displacement due to torsion of the girder.

**Fig. 9** – Displacement of the girder from FEM analysis to find the torsional displacement.

**Fig. 10** – Shape of the STM for the deck, actual strut is bottle shaped.

**Fig. 11** – Stress and strain distribution in a mid-span section of the deck.

**Fig. 12** – Simplification of the STM ( $E_d$  is modulus of elasticity of the deck).

**Fig. 13** – Wisconsin 54in. deep girder.

**Fig. 14** – Modeling of the bridge for parametric study.

**Fig. 15** – Ultimate capacity vs. deck restraining factor for 7.5 in. (191 mm) deep decks with 6 ft. (1829 mm) lateral tie spacing and: (a) Clear deck span = 3 ft. (914 mm); (b) Clear deck span = 4 ft. (1219 mm); (c) Clear deck span = 5 ft. (1524 mm); and (d) Clear deck span = 6 ft. (1829 mm).

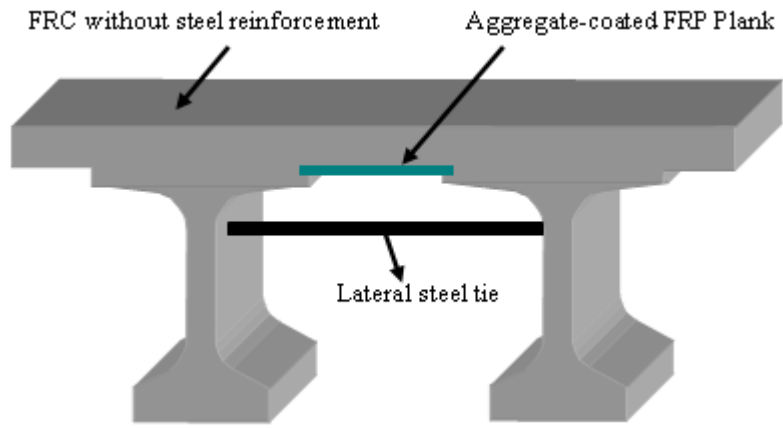


Fig. 1–Reinforcement-free deck concept.

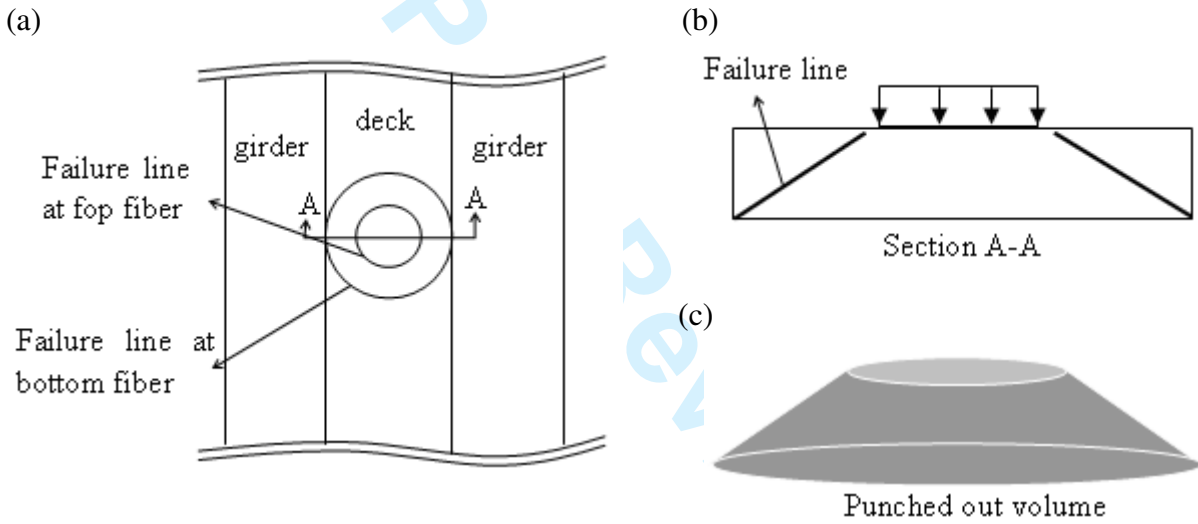
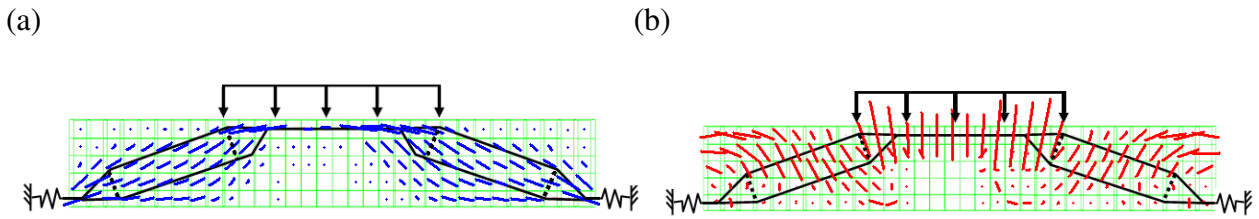
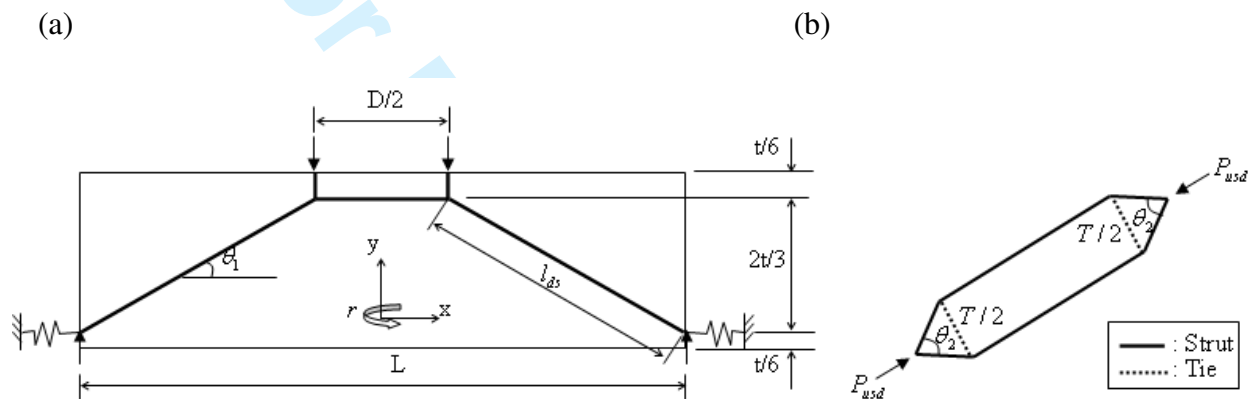


Fig. 2–Failure shape of the punching shear failure at the deck: (a) Plan view of the deck and girder; (b) Section A-A; and (c) Punched out volume



**Fig. 3—Stress trajectory and STM of the deck: (a) Compressive stress trajectory; and (b) Tensile stress trajectory.**



**Fig. 4—STM: (a) Simplified STM for the restrained deck with boundary condition; and (b) Detailed STM of diagonal strut.**

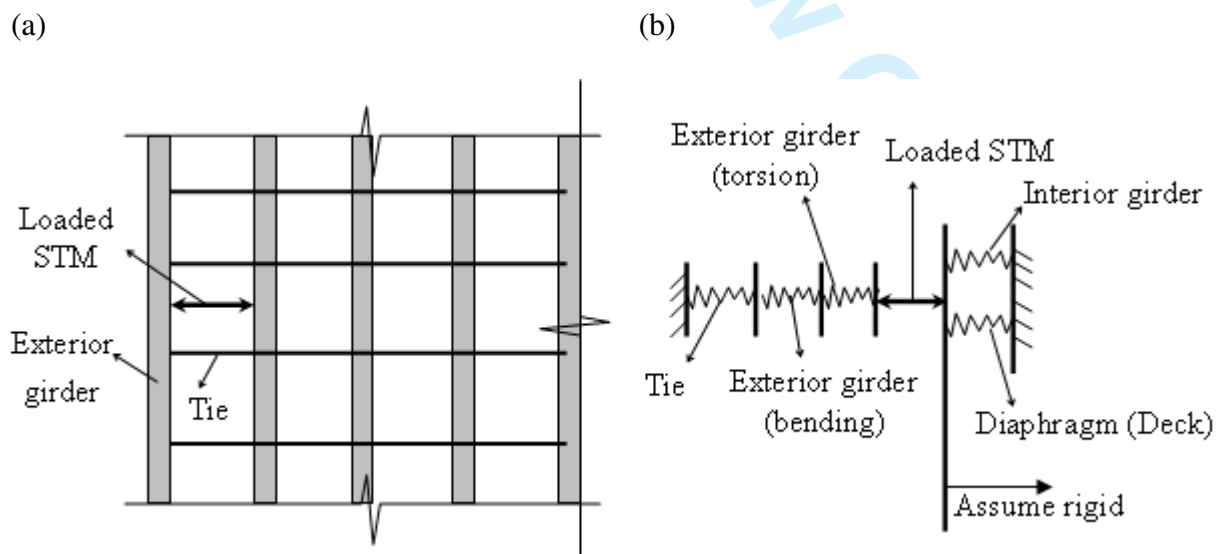


**Fig. 5—Diagram of the lateral stiffness for the STM; (a) Plan view of the deck and girder; and (b) Components of lateral stiffness.**

1  
2  
3  
4  
5  
6  
7  
8  
9  
10  
11  
12  
13  
14  
15  
16  
17  
18  
19  
20  
21  
22  
23  
24  
25  
26  
27  
28  
29  
30  
31  
32  
33  
34  
35  
36  
37  
38  
39  
40  
41  
42  
43  
44  
45  
46  
47  
48  
49  
50  
51  
52  
53  
54  
55  
56  
57  
58  
59  
60

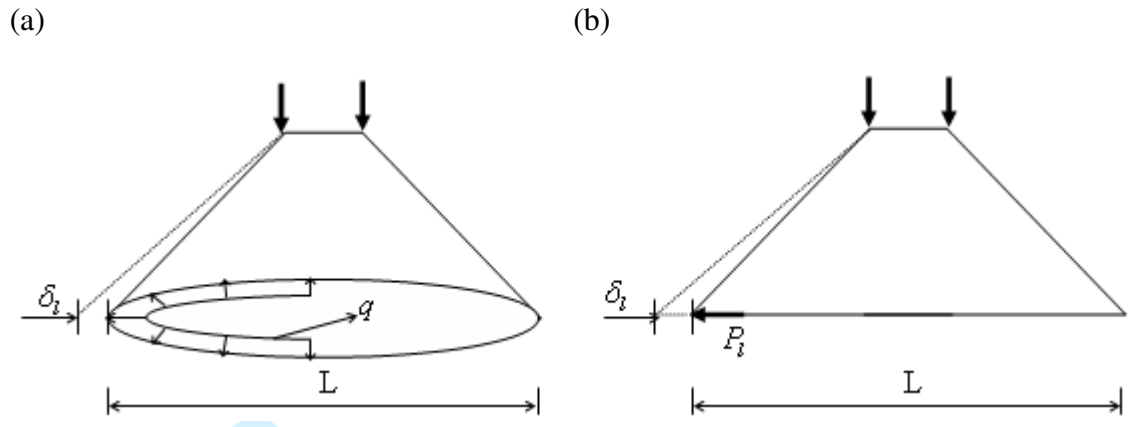


Fig. 6–Diagrams to calculate the spring stiffness of the STM: (a) 3D model; and (b) 2D model.

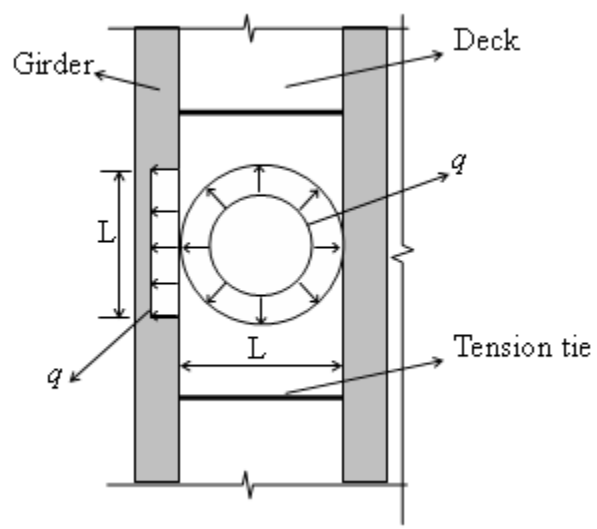


Fig. 7–Distribution of the lateral load acting on the girder.

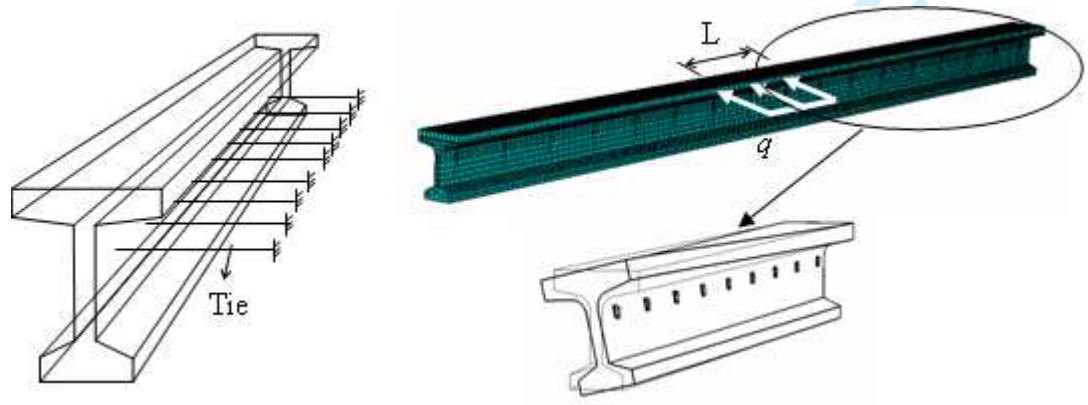


Fig. 8–FEM analysis of the girder to find the lateral displacement due to torsion of the girder.

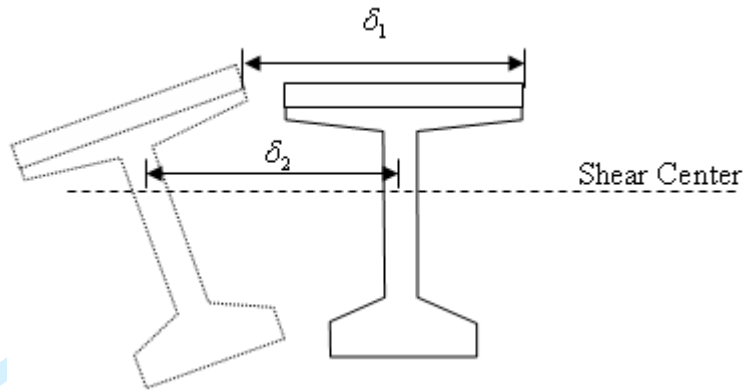


Fig. 9–Displacement of the girder from FEM analysis to find the torsional displacement.

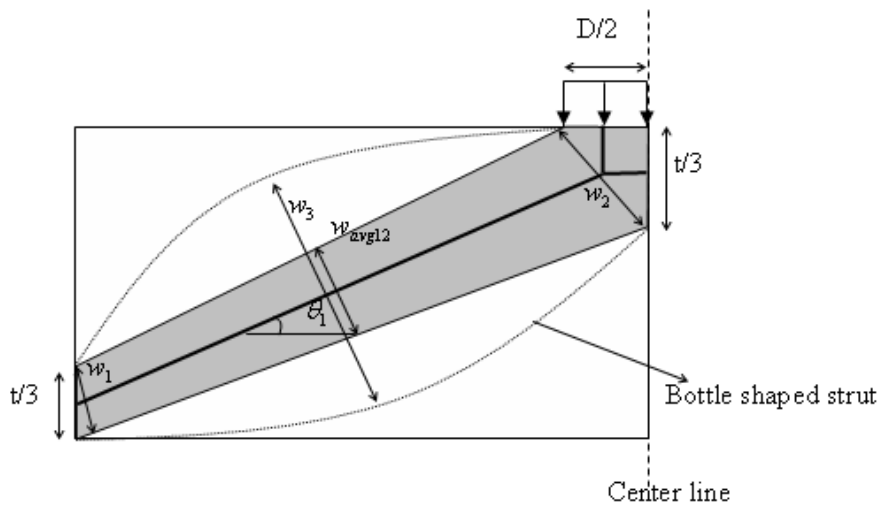


Fig. 10–Shape of the STM for the deck, actual strut is bottle shaped.

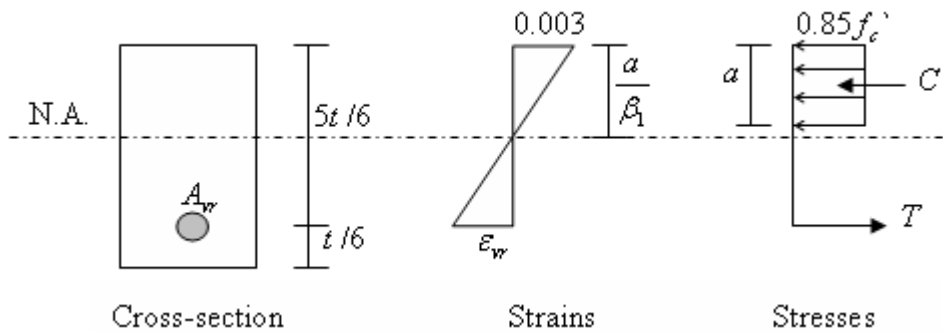


Fig. 11–Stress and strain distribution in a mid-span section of the deck.

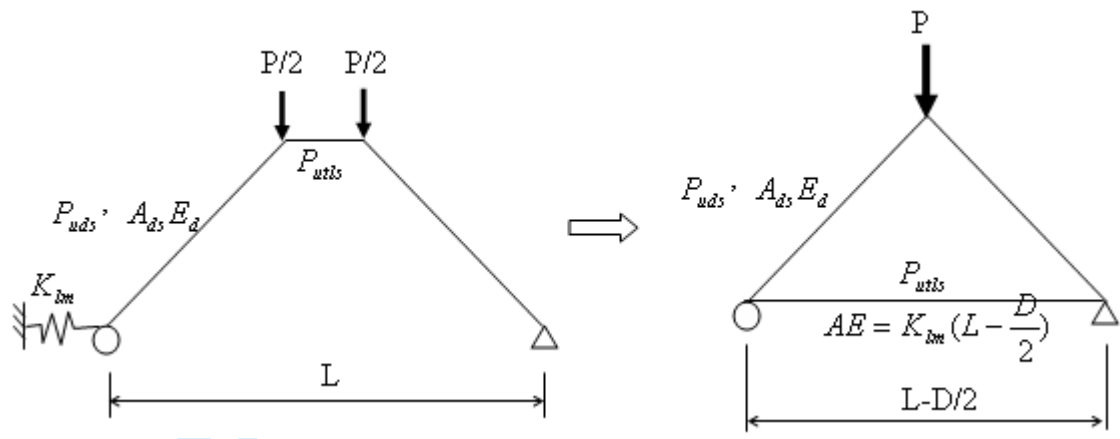


Fig. 12–Simplification of the STM ( $E_d$  is modulus of elasticity of the deck).

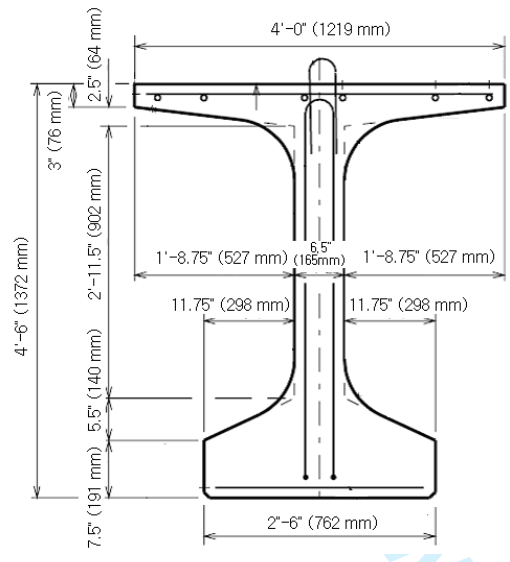


Fig. 13–Wisconsin 54in. deep girder.

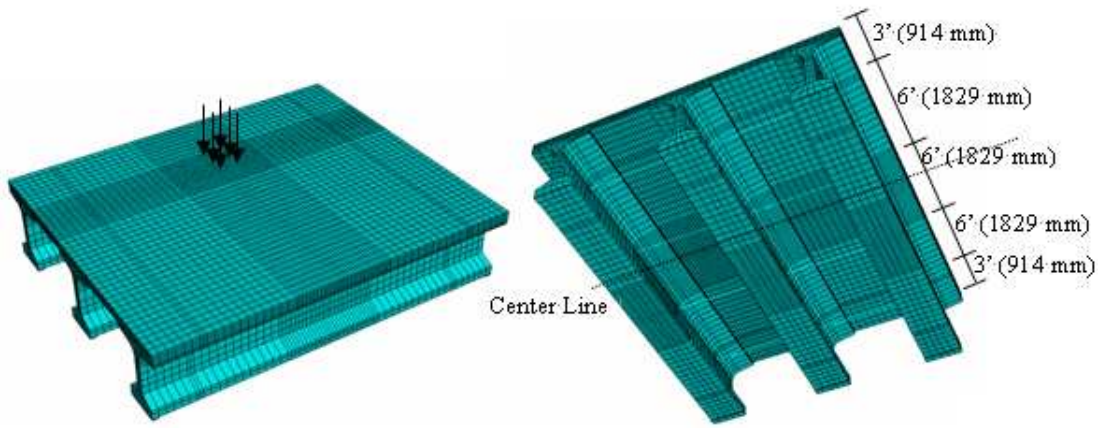
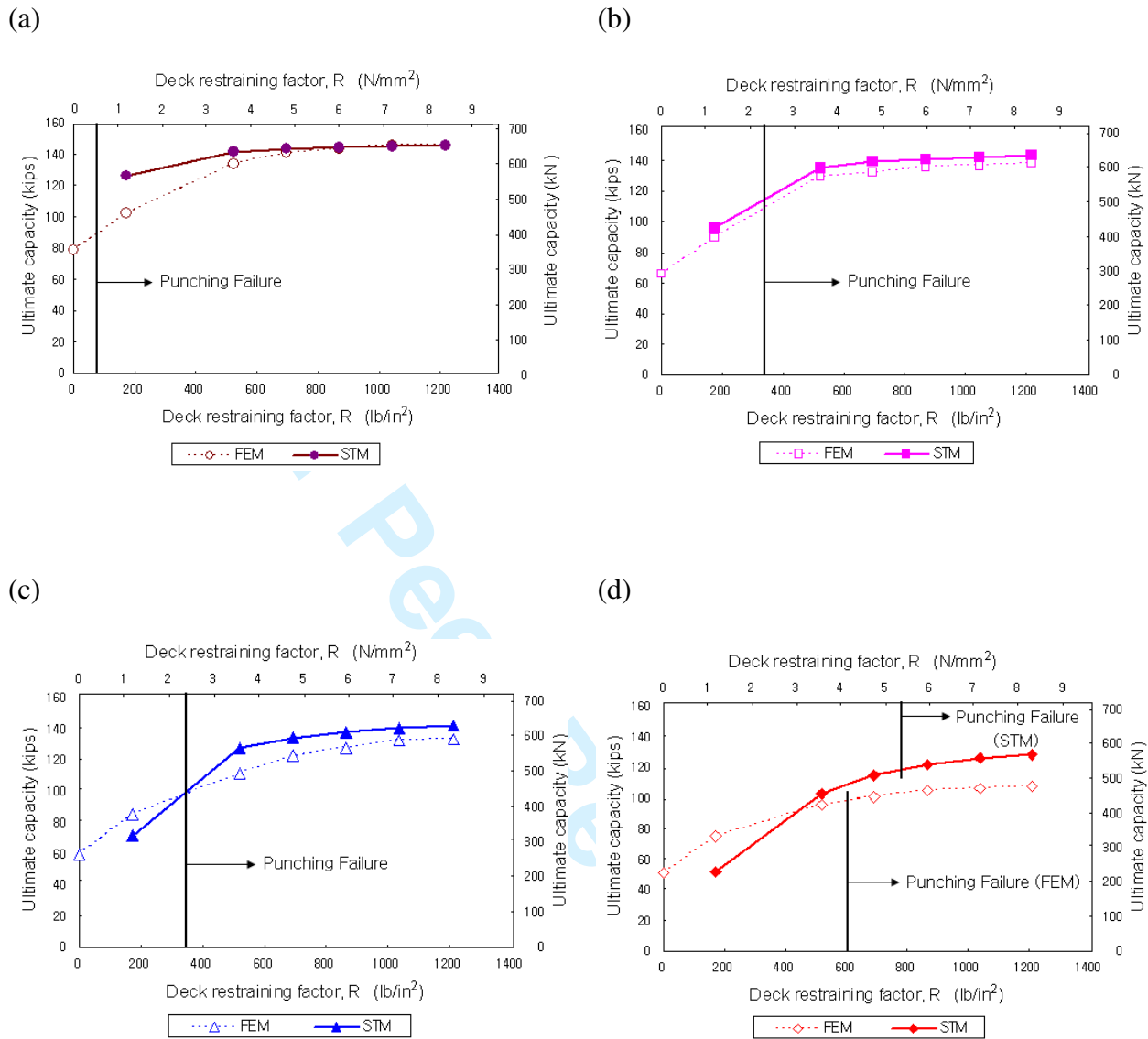


Fig. 14–Modeling of the bridge for parametric study.



**Fig. 15–Ultimate capacity vs. deck restraining factor for 7.5 in. (191 mm) deep decks with 6 ft. (1829 mm) lateral tie spacing and: (a) Clear deck span = 3 ft. (914 mm); (b) Clear deck span = 4 ft. (1219 mm); (c) Clear deck span = 5 ft. (1524 mm); and (d) Clear deck span = 6 ft. (1829 mm).**